Available online at www.sciencedirect.com

ScienceDirect

Procedia Computer Science 181 (2021) 198–205

Procedia Computer Science

www.elsevier.com/locate/procedia

CENTERIS - International Conference on ENTERprise Information Systems / ProjMAN - International Conference on Project MANagement / HCist - International Conference on Health and Social Care Information Systems and Technologies 2020

Persistent Scatterer Interferometry in mountainous areas: advantages of working in map geometry

Christophe Magnard*, Urs Wegmüller, Charles Werner

Gamma Remote Sensing AG, Worbstrasse 225, CH-3073 Gümligen, Switzerland

Abstract

We compare the processing of Persistent Scatterer Interferometry data in map geometry versus their processing in slant-range/azimuth radar coordinates. In mountainous areas, using the map geometry significantly reduces the geometric distortion of radar coordinates that places scatterers that are actually widely separated in altitude in very close proximity in terms of slant-range. Processing in slant-range coordinates over mountainous regions introduces distortion in the distances used for estimation and filtering of tropospheric phase and phase unwrapping. Spatial filtering, interpolation of missing values, and phase unwrapping have better performance in map geometry because the distances between points are closer to reality. Performing these steps in a map geometry results in a more robust and more reliable processing chain.

© 2021 The Authors. Published by Elsevier B.V.
This is an open access article under the CC BY-NC-ND license (https://creativecommons.org/licenses/by-nc-nd/4.0)
Peer-review under responsibility of the scientific committee of the CENTERIS - International Conference on ENTERprise Information Systems / ProjMAN - International Conference on Project MANagement / HCist - International Conference on Health and Social Care Information Systems and Technologies 2020

Keywords: DInSAR; PSI; SBAS; time-series analysis; mountainous terrain; steep topography; filtering in map projection; interpolation in map projection, phase unwrapping in map projection, geographical coordinates; map geometry; SAR geometry; displacement monitoring;

* Corresponding author. Tel.: +41-31-9517005 ; fax: +41-31-9517008 .
E-mail address: magnard@gamma-rs.ch

1877-0509 © 2021 The Authors. Published by Elsevier B.V.
This is an open access article under the CC BY-NC-ND license (https://creativecommons.org/licenses/by-nc-nd/4.0)
Peer-review under responsibility of the scientific committee of the CENTERIS - International Conference on ENTERprise Information Systems / ProjMAN - International Conference on Project MANagement / HCist - International Conference on Health and Social Care Information Systems and Technologies 2020
10.1016/j.procs.2021.01.123

1. Introduction

The analysis of Interferometric Synthetic Aperture Radar time-series using persistent scatterer interferometry (PSI) is a well-established technique for retrieving surface deformation [1,2,3]. This technique builds a field of measurements from the scatterers phase measurement from which surface deformation can be derived. Atmospheric path delay effects and perpendicular baselines in combination with scatterer height inaccuracies result in phase errors and prevent directly obtaining a homogeneous field of deformation measurements. In order to estimate the components of these phase distortions, the behavior of the field of scatterers is analyzed: spatially smooth phase deviations with a height-dependent component but without temporal correlation are most likely caused by atmospheric phase delays; perpendicular baseline-dependent phase deviations are most likely due to errors in the scatterer height information. After their estimation, these phase distortions are subtracted from the interferometric phase. Operations such as spatial filtering, phase unwrapping, and interpolation are used in this estimation process. These operations are typically performed in Synthetic Aperture Radar (SAR) geometry, i.e., with scatterers arranged along slant-range and azimuth coordinates. Applying these operations in SAR geometry can lead to significant processing errors due to spatial distortion. Image regions that differ in altitude can be in very close spatial proximity with areas of radar layover between them. Phase jumps can then occur due to the dependence of the atmospheric path delay component on the topographic height.

In this article, we investigate the effect of performing spatial filtering, phase unwrapping, and interpolation of missing values in a map geometry. The term “map geometry” here includes both map projections (easting / northing) and geographic coordinate systems (latitude / longitude). A stack of Sentinel-1 data acquired over a high alpine area is used to compare results processed in both SAR and map geometries. The focus of this work is not on a specific time-series analysis and presentation of results, but on the investigation and assessment of improvements achieved in specific steps used in such a sequence.

The article is organized as follows: in Section 2, we shortly describe the application case used. Then in Section 3 we describe the methods compared, e.g. spatial filtering in SAR geometry versus spatial filtering in map geometry, the tests conducted to assess the methods, the results achieved in these tests, and the improvement achieved. Finally, conclusions and recommendations are provided in Section 4.

2. Test site and data

As an example for the measurement of deformation due to a landslide, a stack of 25 Sentinel-1 scenes is used. These were acquired during the snow-free period in summer and fall 2019 over the high alpine Aletsch area in the Swiss Alps. One of the main objectives of this example is to retrieve information for fast and non-uniform displacements. Consequently, a multi-reference stack with exclusively short (6 to 18 days) temporal intervals was selected that demonstrated relatively high temporal and spatial coherence. A combination of both point-like persistent scatterers and distributed scatterers could be used. The size of the investigated area is 15 km × 21 km with altitudes varying between 700 and 4100 m. Fig. 1a shows the geocoded SAR image and Fig. 1b shows the height projected into SAR slant-range/azimuth geometry. The time-series analysis is done for selected persistent scatterer candidates including single-look and multi-look (about 15 range x 3 azimuth looks) elements. Based on the spectral correlation criteria used in the candidate selection [3,4] the single-look elements correspond primarily to point-like scatterers. The multi-look elements are used to get good coverage in areas with primarily distributed scatterers. Fig. 2 shows, for a small subset of the complete scene, the single-look and multi-look elements included in the final solution. Notice the heterogeneity of the spatial sampling with large spatial gaps due to radar layover.

For further information on the processing sequence that was used and the results see [5]. We focus in this report on the improvement of a few specific processing steps.

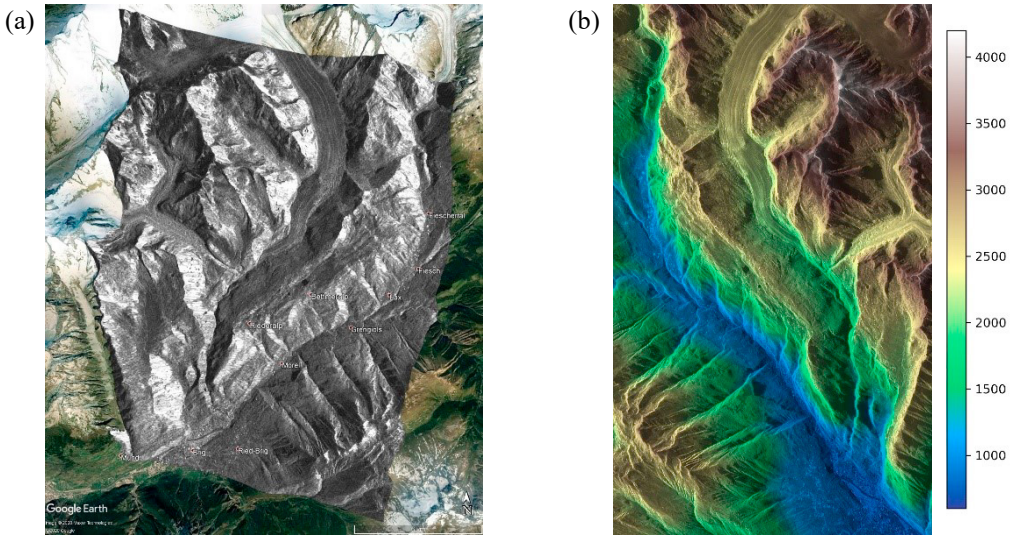
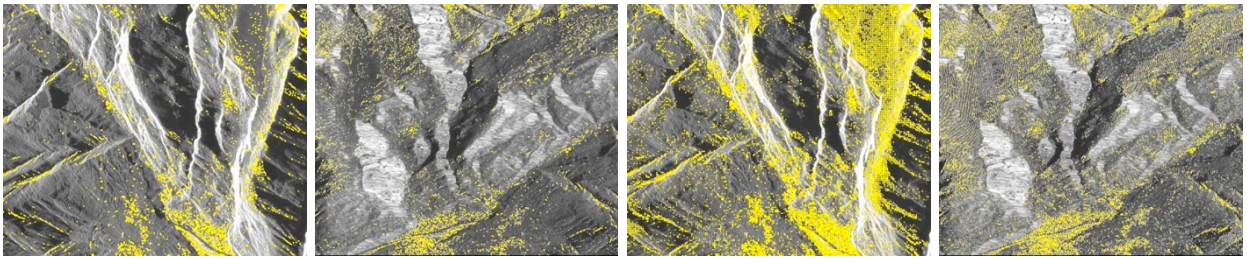


Fig. 1. (a) Geocoded average SAR image overlaid on Google Earth image. (b) Height in slant-range geometry (meter above WGS84 ellipsoid).



a) single-look, slant-range geometry b) single-look, map geometry c) all, slant-range geometry d) all, map geometry

Fig. 2 For a small subset, the single-look elements (a,b) and all elements (point and distributed scatterers) (c,d) are shown in SAR slant-range and in map geometry. High densities of single-look elements are found in built-up areas. Including multi-look elements strongly increases the spatial coverage in sparsely vegetated areas, in this case mainly above the forest line.

3. Processing steps performed in map geometry vs. SAR geometry

In this section, spatial filtering, interpolation of missing values, and phase unwrapping tests were performed in both map and SAR geometry. These tests were designed to be close to how the PSI processing tools are used in practice and to ensure a fair comparison.

Clear differences in the results are shown in point data images. In the spatial filtering and interpolation tests, we also calculate the standard deviation of the phase difference between the filtered / interpolated phase and the original phase. While one should not focus on the absolute value of this standard deviation, comparing the standard deviations obtained when processing in map vs SAR geometry shows to what degree the phase is skewed by processing.

3.1. Spatial filtering

Spatial filtering is used both for estimation of atmospheric phase and to improve phase unwrapping. Spatial filtering is performed by averaging the data associated to a point (e.g. phase values) with the data of the neighbor points found within a specified radius. In the SAR geometry processing sequence, distances are calculated in meters in a ground range / azimuth frame, such that for flat areas, results are essentially the same as in map geometry. Various weighting functions can be used for the spatial averaging, including rectangular, triangular or gaussian distance weighting

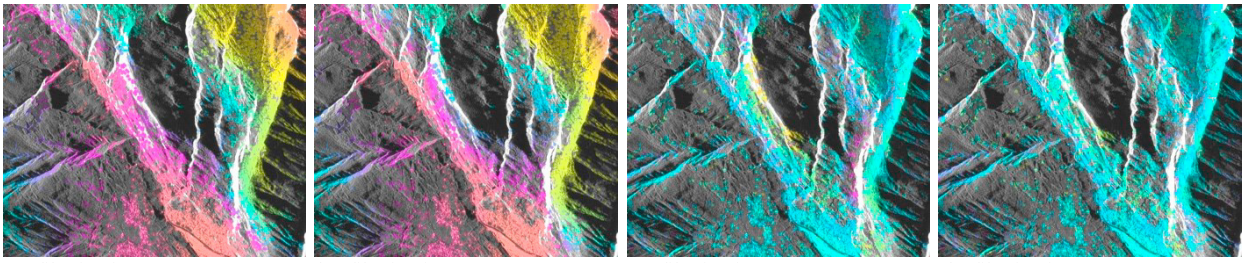
functions. The filtering kernel radius depends on the purpose of the filtering: the radius will typically be in a kilometer-scale for filtering done in the estimation of the atmospheric path delay phase, and in tens to hundreds of meters scale as a pre-processing step for phase-unwrapping.

In the following, we compare filtering results using rectangular, uniform-weighted windows of different sizes. In the SAR geometry case, the indicated filter radius corresponds to the radius in ground-range to make the comparisons transparent.

The unfiltered atmospheric phase is obtained by masking out elements that show deformation or low temporal coherence, followed by spatial filtering and interpolation. An example is shown in Fig. 3 for a single interferometric pair with a filter radius of 1 km. We observe that when filtering in SAR geometry, points in the valley are averaged together with points from the mountain tops, significantly skewing the results when compared with the map geometry. This effect is also visible (Fig. 4a) when plotting the standard deviation of the phase difference relative to the filter radius. While the magnitude error varies for the different interferograms, all interferograms had better statistics when filtered in map geometry with a 1 km filter radius, as shown in Fig. 4b.

The same behavior was observed using a triangular weighting window, yielding superior results when filtering in the map geometry. Lower standard deviations were measured in both SAR and map geometries compared to the uniform window. The same behavior was observed using smaller filter windows, for the case of spatial filtering of the differential phase prior to phase unwrapping. With smaller windows, the differences between filtering in SAR and map geometry were reduced, as expected.

A straightforward approach to minimize such issues is to first subtract a height dependent atmospheric phase model from the data prior to filtering. While the magnitude of the error decreases for both cases, filtering of the data in map geometry gives results with significantly lower errors, as shown in Fig. 5.



a) filtering in SAR geometry b) filtering in map geometry c) filtering in SAR geometry, difference with unfiltered data d) filtering in map geometry, difference with unfiltered data

Fig. 3. For the same image subset as in Fig. 2, the results of filtering the atmospheric phase are shown when performed in SAR geometry (a) and in map geometry (b), as well as the respective difference with the unfiltered data (c, d). The color scale is cyclical over 4π. The results are shown in SAR slant range geometry, to show the differences in a common geometry.

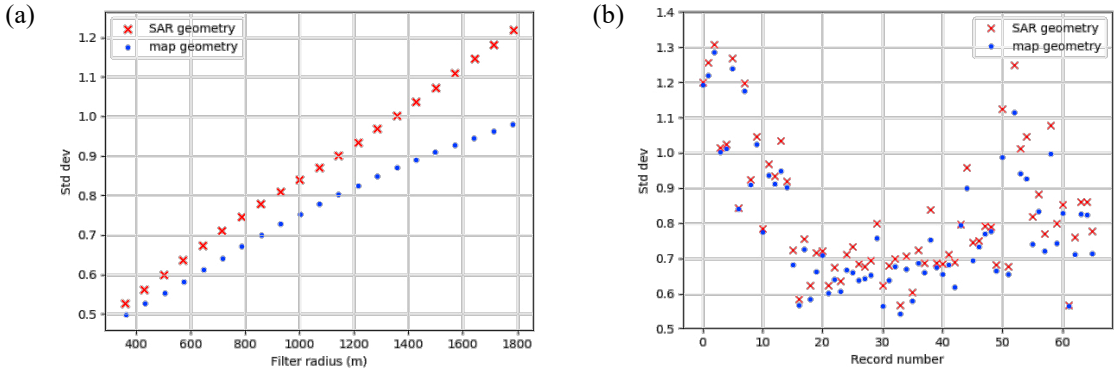


Fig. 4. (a) Standard deviation of the difference between the unfiltered and filtered phase for one interferometric pair and various filter sizes (b) Standard deviation of the difference between the unfiltered and filtered phase for each interferometric pair using a filter with a 1 km radius.

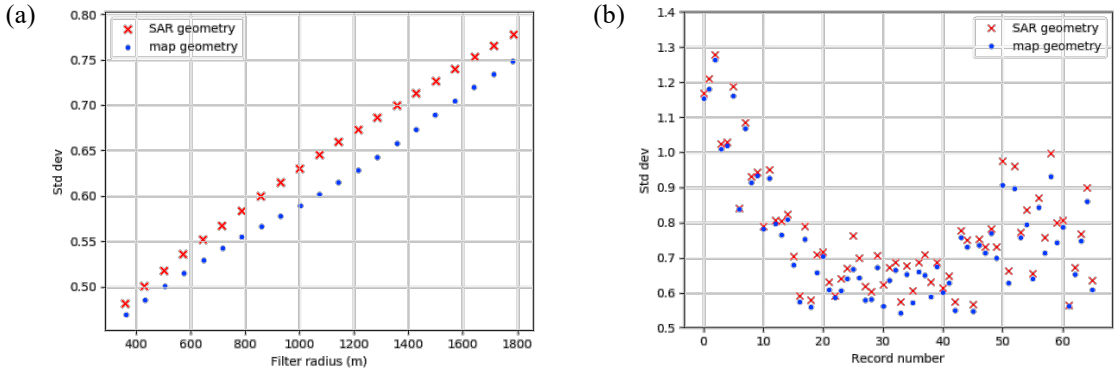


Fig. 5. Same plots as in Fig. 4; here a height dependent atmospheric phase model was subtracted from the input phase prior to filtering.

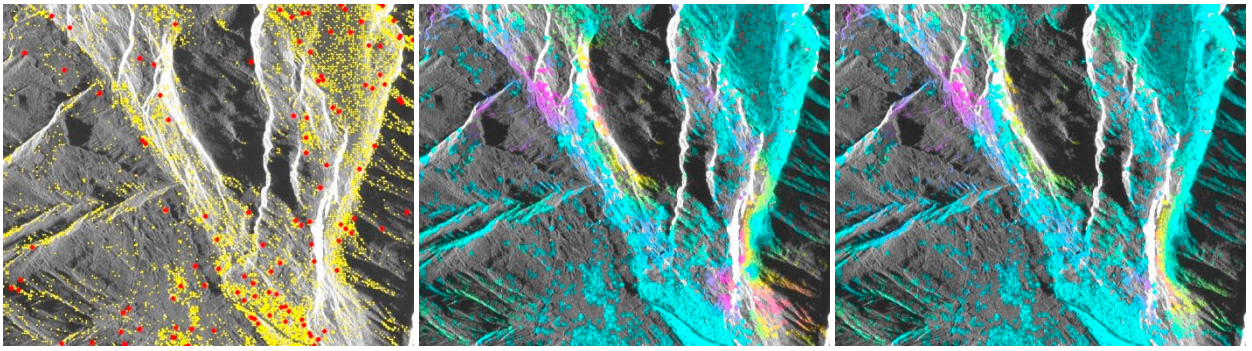
3.2. Interpolation of missing values

Interpolation of missing values is used to estimate values for points that were masked or discarded in a previous step. For example, the atmospheric path delay phase can be interpolated for isolated points or point clusters that had to be discarded previously. When calculating the atmospheric phase for cases with localized, rapid deformation, points expected to contain a deformation signal may be masked, and the atmospheric phase has to be interpolated for those points. Another case is when points showing excessive standard deviation are discarded, e.g. due to phase unwrapping errors: after subtraction of the interpolated atmospheric phase, these points may show improved statistics and then be reintegrated into the set of points with an accepted solution.

Spatial interpolation can be done in number of ways. One approach is to generate a regular grid where the pixel values on the grid are computed using a distance weighted average of the neighboring points. The regular grid is then filled in completely using inpainting [6,7]. The point values are subsequently interpolated from the grid using a bicubic B-Spline interpolator [8,9].

As a test, we discarded 99% of the points and interpolated their values in both SAR and map geometries. The interpolation is used to fill relatively large gaps, e.g. masked deformation areas or wrongly unwrapped point clusters that were rejected. Randomly discarding such a large proportion of points creates gaps on a similar scale. The remaining points can be seen in red in Fig. 6a, while the interpolated points are shown in yellow. The data used for the interpolation test was the filtered atmospheric phase, i.e., the unwrapped phase residuals that had been filtered using a uniform 1 km filter radius. In order to perform a fair comparison between the SAR and map geometry versions, a similar intermediate interpolation grid was used, i.e., using similar pixel spacings (123.55 m in map geometry, 125.19 m in SAR geometry). The differences between the original and the interpolated values when interpolating in SAR and map geometry are displayed in Fig. 6b and Fig. 6c respectively for a subset of an interferometric pair. We clearly see that the points interpolated using the map geometry are less skewed than those interpolated using the SAR geometry.

The standard deviation of the difference between the original and interpolated atmospheric phase values is shown in Fig. 7 for each interferometric pair. Other input data and interpolation grids were tested; while the absolute values differ, the values interpolated in map geometry always showed lower differences relative to the original data compared to the values interpolated in SAR geometry.



a) points shown in SAR geometry b) results of the SAR geometry interpolation c) results of the map geometry interpolation

Fig. 6. The support points for the interpolation (red) and the interpolated points (yellow) are shown in (a). The differences between the original and the interpolated values for one interferometric pair using interpolation in SAR geometry and in map geometry are shown in (b) and (c), respectively. A cyclical color scale over 2π was used. The results are shown in SAR slant range geometry.

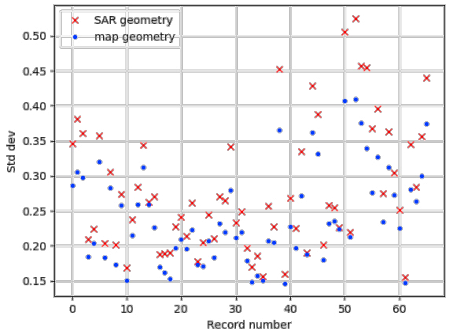


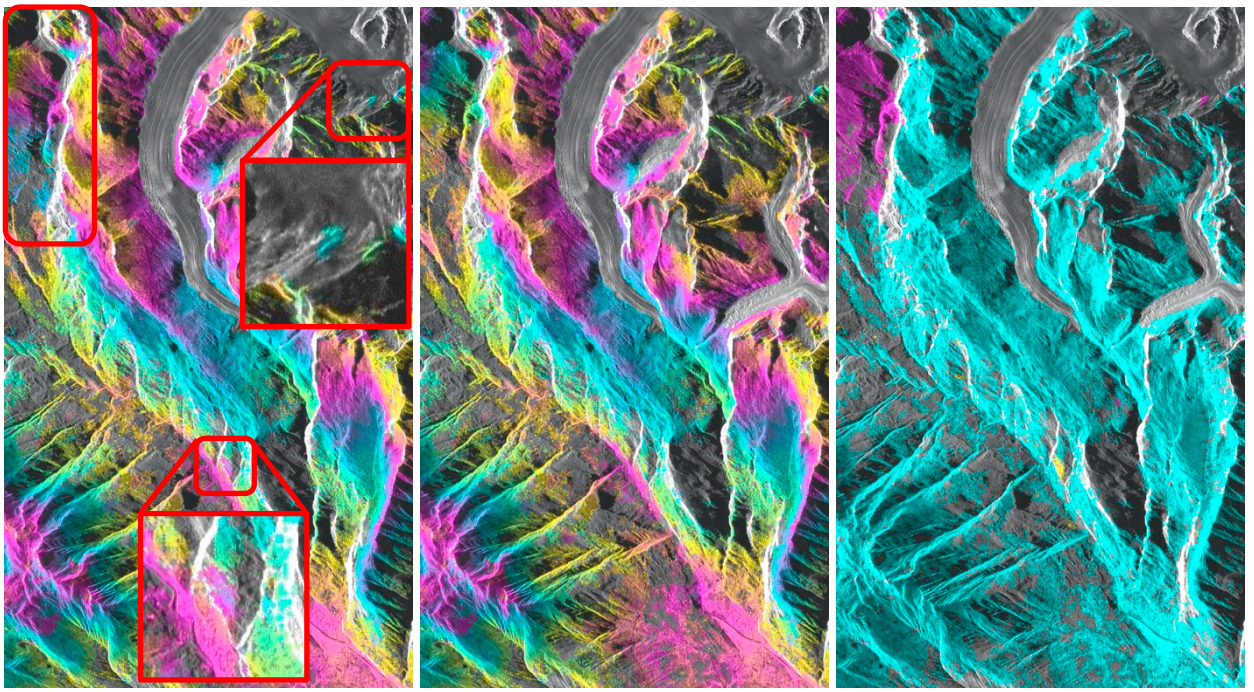
Fig. 7. Standard deviation of the difference between the original and interpolated atmospheric phase values for each interferometric pair.

3.3. Phase unwrapping for point data stack using Minimum Cost Flow algorithm

The method used in our investigation was the Minimum Cost Flow (MCF) phase unwrapping algorithm [10,11], as implemented in the GAMMA Software [4]. Its implementation uses a Delaunay triangulation [12]. In the algorithm used for this study, phase unwrapping is applied to the rewrapped and filtered residuals from the regression analysis on the spatio-temporal phase differences [5]. It could also be used directly on the original stack of differential phases, with or without filtering, and the result could then be used to estimate a first height-dependent atmospheric path delay model.

While weights such as spatial coherence values are typically provided to the MCF algorithm for unwrapping an interferogram in a regular grid, spatial coherence may not be available or desirable for unwrapping point data. Temporal coherence could be used in a second iteration, i.e., after a first deformation result has been obtained for the whole point data stack. Alternatively, other weighting schemes could be considered, e.g. relying on the distance between the points, the size of the triangles, or the variability of the height within the triangles.

The MCF phase unwrapping was performed on the rewrapped and filtered residuals both in map and SAR geometry, using constant weights. Fig. 8 shows the phase unwrapping results for one interferometric pair. Fig. 8a was unwrapped in SAR geometry, while Fig. 8b was unwrapped in map geometry. Fig. 8a includes several areas with phase unwrapping errors (marked in red), while Fig. 8b seems to have been unwrapped correctly. The difference (φ_{SAR} - φ_{map}) is shown in Fig. 8c, where the phase unwrapping differences are clearly visible.



a) MCF in SAR geometry b) MCF in map geometry c) phase difference between (a) and (b)

Fig. 8. Unwrapped residuals using MCF in SAR (a) and map (b) geometry for one interferometric pair. The larger phase unwrapping differences are marked in red. The color scale is cyclical over 4π. The difference (φ_{SAR} - φ_{map}) is shown in (c), purple is $+2\pi$, yellow is -2π and turquoise is 0. The results are shown in SAR slant range geometry.

In the Aletsch example, some interferometric pairs seem to be correctly unwrapped in both SAR and map geometry while others include errors when unwrapped in SAR geometry. No major errors seem to have occurred when unwrapping in map geometry, though it is sometimes difficult to assess the result with full confidence.

4. Conclusions and discussion

Time series analysis of persistent scatterers in mountainous areas performed in SAR geometry can be complicated due to the combination of the foreshortening effect with strong height-dependent atmospheric phase distortion. The results presented in Section 3 show that performing a set of processing steps in map geometry, i.e., spatial filtering, phase unwrapping, and interpolation of missing values, provides substantial advantages compared to a processing done solely in SAR geometry. These advantages are documented in Section 3 on one hand through the examples that show obvious improvements when doing the steps in map geometry and on the other hand through the produced statistical results. There is a significant improvement when using the map geometry for phase unwrapping due to the elimination of foreshortening and layover distortion. As a consequence, more points could be included in the final result with improved temporal coherence.

While work-around methods may be found to reach similar results when working in SAR geometry, performing the processing in map geometry results in a simplified, reliable, and robust process.

Aside from the discussed filtering, interpolation, and phase unwrapping steps, other steps may benefit from using map geometry. In particular the development of the PSI solution along a network, or as done in the GAMMA Software using smaller patches and then using patch-to-patch connections is expected to benefit. Designing the network in the map geometry will put far apart points on mountain tops and valleys that are close to each other in SAR geometry. In map geometry, the network will therefore not have direct connections between such difficult to connect point pairs, making the development of the solution more robust.

Acknowledgements

ESA/Copernicus are acknowledged for the Sentinel-1 data used.

References

[1] Ferretti, A., C. Prati, and F. Rocca, "Permanent scatterers in SAR interferometry," *IEEE Transactions on Geoscience and Remote Sensing*, vol. 39, no. 1, pp. 8–20, Jan. 2001.

[2] P. Berardino, G. Fornaro, R. Lanari, and E. Sansosti, "A new algorithm for surface deformation monitoring based on small baseline differential SAR interferograms," *IEEE Transactions on geoscience and remote sensing*, vol. 40, no. 11, pp. 2375–2383, 2002.

[3] Wegmüller U., C. Werner, T. Strozzi, and A. Wiesmann, "Multi-temporal interferometric point target analysis," in *Analysis of Multi-temporal remote sensing images*, Smits and Bruzzone (ed.), Series in Remote Sensing, Vol. 3, World Scientific (ISBN 981-238-915-61), pp. 136-144, 2004.

[4] Gamma Software Information, 2020; https://www.gamma-rs.ch/uploads/media/GAMMA_Software_information.pdf.

[5] Wegmüller, U., C. Magnard, C. Werner, T. Strozzi, R. Caduff and A. Manconi, "Methods to avoid being affected by non-zero closure phase in InSAR time series analysis in a multi-reference stack," submitted to *Procedia Computer Science*, 2020.

Note: This article has also been submitted to the SARWatch 2020 conference

[6] Bertalmio, M., G. Sapiro, V. Caselles, and C. Ballester, "Image inpainting," in *Proceedings of the 27th annual conference on Computer graphics and interactive techniques*, pp. 417-424, 2000.

[7] D'Errico, J. (2004). Inpaint_nans. www.mathworks.com/matlabcentral/fileexchange/4551-inpaint-nans

[8] Unser M., A. Aldroubi, and M. Eden, "B-Spline Signal Processing: Part I-Theory," *IEEE Transactions on Signal Processing*, vol. 41, no. 2, pp. 821-832, 1993.

[9] Unser M., A. Aldroubi, and M. Eden, "B-Spline Signal Processing: Part II-Efficient Design and Applications," *IEEE Transactions on Signal Processing*, vol. 41, no. 2, pp. 834-848, 1993.

[10] Werner, C., U. Wegmüller, T. Strozzi, and A. Wiesmann. "Processing strategies for phase unwrapping for INSAR applications," in *Proceedings of the European Conference on Synthetic Aperture Radar (EUSAR 2002)*, vol. 1, pp. 353-356, 2002.

[11] Costantini, M, "A novel phase unwrapping method based on network programming," *IEEE Transactions on geoscience and remote sensing*, vol. 36, no. 3, pp. 813-821, 1998.

[12] M. Bern and D. Eppstein, "Mesh Generation and Optimal Triangulation," in *Computing in Euclidean Geometry*, Ding-Zhu Du and Frank Hwang (eds.), World Scientific, Singapore, pp. 23-90, 1992.